IEEE Access
Multidisciplinary | Rapid Review | Open Access Journal

Date of publication xxxx 00, 0000, date of current version xxxx 00, 0000.

Digital Object Identifier 10.1109/ACCESS.2024.Doi Number

Data-driven Compensation Algorithm for Optimizing Power Quality in Interleaved Boost PFC

Cong Li[1], Qi Zhang[1], *Member*, *IEEE*, Rongwu Zhu[2], *Senior Member*, *IEEE*, Jiahao Zhang[1], Hui Yang[1], Fujin Deng[3], *Senior Member*, *IEEE*, Xiangdong Sun[1], *Member*, *IEEE*

[1]School of Electrical Engineering, Xi'an University of Technology, Xi'an 710048, China
[2]Department of Electrical Engineering, Harbin Institute of Technology, Shenzhen 518055, China
[3]School of Electrical Engineering, Southeast University, Nanjing 210096, China

Corresponding author: Qi Zhang (e-mail: zhangqi@xaut.edu.cn).

This work was supported in part by the National Key Research and Development Program of China under Grant 2022YFE0196300, in part by the Talent Recruitment Project of Guangdong under Grant 2021QN02L474, in part by the Major project of Natural Science Foundation of Shenzhen-the Stable Support Plan Program under Grant GXWD20220819112051004, in part by the Youth Innovation Team of Shaanxi Universities.

ABSTRACT Nonlinearities of inductor's soft magnet, converter's time-varying mode and control delays limit the grid-side power quality improvement capability of interleaved boost Power Factor Correction (PFC) circuit. The traditional internal model principle-based approaches are widely used to improve the power quality, but the expense is the reduce of certain stability. Hence, this paper proposes a data-driven online compensation method to address this trade-off between control accuracy, power quality and stable margin. This method involves recording control data of a multi-frequency proportional resonant (PR) controller under various input conditions. The collected data is preprocessed and used to establish a regression compensation model through multivariate nonlinear regression. Finally, this regression model is applied to the compensation loop of a lower-order controller to improve power quality of the PFC while ensuring sufficient stable margin. Experiments verify the practical feasibility and the effectiveness of the proposed data-driven control method.

INDEX TERMS Power factor correction, soft saturation characteristics, data-driven, multivariate nonlinear regression.

I. INTRODUCTION

Power factor correction circuits (PFCs) are extensively used in electrical appliances to mitigate harmonic pollution and minimize reactive power losses, thereby facilitating the seamless integration into the power grids [1-2]. The performances of typical digital controllers for PFC are often constrained by multiple factors, in particular of the nonlinearities caused by the power semiconductors, magnet and delay. The power quality improvement of PFC has become one of most important concerns.

The increase of inductance can effectively improve the grid power quality, but lead to the higher hardware costs and potential risk of bus overshoot during the unloading instants [3]. The selection of magnetic inductors with high saturation can lower hardware costs while reduce stable margin [4]. The improvement of controllers is often accompanied by an increase in system complexity, which may introduce additional computational demands and orders of system control model [5]. Furthermore, increasing the bus voltage response capability leads to a degradation in the grid current quality due to the cross-limitation between the control loops of voltage and current [6]. Therefore, the control challenges faced by PFC still require continuously to be addressed.

The comprehensive optimization of system cost and power quality as well as power density has been conducted from the perspective of improving the topology structure. The fundamental analysis of the essential circuit properties of different topological structures were provided in [7]. By adding extra branches, the current ripple of the interleaved boost converter (IBC) is reduced. Additionally, due to the

decrease of inductance and power diversion, the system exhibits comprehensive cost advantages in specific scenarios. The addition of interleaved branches can further enhance power quality, but it requires a balance between cost, reliability and requirements for power quality [8]. The implementation of auxiliary circuits in IBC-PFC to enable soft-switching and reduce switching losses is being investigated [9-10]. However, the inclusion of additional auxiliary circuits presents challenges for its industrial application.

In the absence of auxiliary circuits, improvements in modulation techniques such as discontinuous current mode (DCM) [11], boundary current mode (BCM) [12-13], transition current mode (TCM) [14], and their hybrid variations [15-16, 25] have been investigated to achieve soft-switching characteristics and enhance power density in various applications. However, reducing the inductance value to achieve these benefits leads to increased ripples of current. Additionally, there is a trade-off between stable margin and control gain when employing linear controllers [6]. To address this, analog controller such as hysteresis control [17-18] or hybrid control of analog and digital methods [19] are utilized, resulting in the increased complexity of the controllers.

Recent years，the emergence of data-driven science has provided a new perspective for addressing the aforementioned problems. Model predictive control (MPC), which is an impactful application of data-driven approaches, involves real-time forecasting based on limited numbers of input and state feedback. It continuously optimizes control outputs in accordance with constraint conditions. In [20], the dynamic adjustment of weighting coefficients is achieved through the combination of increasing the weighting factor of the cost function and leveraging artificial intelligence (AI) algorithms. By combining the adaptive moth-flame optimization (MFO) with MPC as described in [21], rapid and precise parameter identification is accomplished. Training with artificial neural networks (ANN) based on the data from offline experiments and simulation, in conjunction with MPC, allows for the dynamic adjustment of weighting coefficients to enhance dynamic response capability and control accuracy [22]. However, the utilization of such methodologies, which primarily rely on data derived from linear models, falls short in providing a robust explanation for the underlying data generation mechanism. Furthermore, the quantitative evaluation of stability in these approaches poses considerable difficulties.

The lookup table (LUT) has shown the significant potentials in improving power quality. The LUT, based on the 2k-step summation equation [23], effectively mitigates the non-linearity problems associated with the zero crossing. By incorporating the parasitic capacitance, device voltage drops, dead-time and switching delay into the LUT and using a three-dimensional linear interpolation, the compensation accuracy can be improved [24]. The PFC hybrid modulation

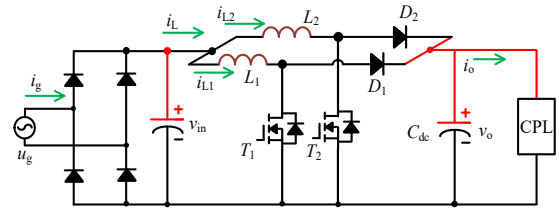

FIGURE 1. Topology of interleaved parallel Boost PFC.

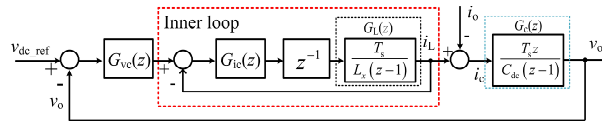

FIGURE 2. Dual-loop control structure of Boost PFC.

mode uses the LUT to achieve optimal mode transition, improving efficiency at low currents and reducing inductor volume [25]. Pre-storing multiple LUTs [26-27] allow the use of more accurate and complex models to improve control accuracy and reduce current harmonics. However, LUTs lack specific application models and the inclusion of additional operating conditions often requires more data storage.

Hence, it is imperative to address the following concerns when implementing data-driven control in power converters: 1) The selected data should possess the capability to yield informative insights into the converter mechanism. 2) The data should be capable of being transformed into mathematically deployable models. 3) It is convenient to implement via the traditional commercial controllers. In this paper, a data-driven online compensation strategy is proposed, and the main contributions of this paper include:1) Training the data using the conventional internal model control method, with a well-defined data training trajectory, ensures its credibility. 2) The data are preprocessed and a data-driven model is obtained using a multivariate nonlinear regression technique, which optimizes the compensation accuracy and data storage efficiency. 3) Combining the regressed data model with the traditional low-order controller to alleviate the contradiction between the dynamic response and the steady state accuracy. Furthermore, the feasibility and effectiveness of this principle based lightweight data-driven method are studied.

The rest of paper is organized as follows: Section II examines the limiting factors imposed on linear controllers applied to PFC. Section III proposes a data-driven based control method for the PFC power quality optimization. Section IV analyzes the applicability of the proposed method. Section V provides experimental validation to demonstrate the feasibility and effectiveness of the proposed method. Finally, conclusions are drawn in Section VI.

II. ANALYSIS OF PFC GAIN MUTUAL LIMITING MECHANISM AND OPTIMIZATION MEASURES

Fig.1 depicts the topology of the IBC-PFC. Here, the grid-side voltage u_g is rectified and then serves as the input voltage v_{in} for the boost circuit. i_g is the grid-side current, i_{L1} and i_{L2}

are the currents of two interleaved inductors, respectively. i_o is the load current, and the load usually exhibits constant power load (CPL) characteristics. v_o is the output DC voltage. Two identical PR controllers are utilized for the control of two interleaved circuits to realize current shaping.

A Control Gain Limitation in PFC

Fig.2 shows the traditional dual-loop control structure of the PFC. The red dashed part is the inner control loop, which includes the current controller $G_{ic}(z)$, the digital control delay z^{-1}, and the discrete model of the inductor $G_L(z)=T_s/[L_x(z-1)]$ (x=1, 2). $G_{vc}(z)$ is the voltage controller used to generate the current reference for the inner loop, ensuring that v_o follows the reference signal v_{dc_ref}. $G_c(z)= T_sz/[C_{dc}(z-1)]$ is the discrete model of the capacitor. k_{pi} and k_{pv} are the global control gains of the two loops $G_{ic}(z)$ and $G_{vc}(z)$, which can be standardized by γ and κ, as shown in (1) [6].

$$\begin{cases} \gamma = \left(k_{pv} T_s\right) / C_{dc} \\ \kappa = \left(k_{pi} T_s\right) / L_x \end{cases} \tag{1}$$

Considering only the global gain κ, the inner loop transfer function is derived as shown in (2).

$$G_{in}(z) = \frac{k_{pi} \cdot T_s}{L_x \cdot \left(z^2 - z\right) + k_{pi} \cdot T_s} = \frac{\kappa}{z^2 - z + \kappa} \tag{2}$$

It is known that the necessary and sufficient conditions for stability of the current loop are obtained as shown in (3) [6], and κ should be within (0, 1) to ensure the current loop stable.

$$\begin{cases} \Delta_{in}(z) = z^2 - z + \kappa \\ 1.\ \Delta_{in}(1) = \kappa > 0 \\ 2.\ (-1)^2 \Delta_{in}(-1) = 2 + \kappa > 0 \\ 3.\ |\kappa| < 1 \end{cases} \tag{3}$$

Furthermore, the system transfer function can be written as (4). Accordingly, (5) must be satisfied to make system stable.

$$G_{Loop}(z) = \frac{\gamma \cdot \kappa \cdot z}{z^3 - 2z^2 + (1 + \kappa + \gamma \cdot \kappa) \cdot z - \kappa} \tag{4}$$

$$\begin{cases} \Delta_{Loop}(z) = z^3 - 2z^2 + (1 + \kappa + \gamma \cdot \kappa) \cdot z - \kappa \\ 1.\ \Delta_{Loop}(1) = \gamma \cdot \kappa > 0 \\ 2.\ (-1)^3 \Delta_{Loop}(-1) = 4 + 2\kappa + \gamma \cdot \kappa > 0 \\ 3.\ |\kappa| < 1, \text{ and } \left|1 - \kappa^2\right| > \left|1 + \gamma \cdot \kappa - \kappa\right| \end{cases} \tag{5}$$

Based on (5), the constraints and ranges of the global gains are derived in (6), and the coupling relationship between k_{pi} and k_{pv} is illustrated in (7). Specifically, as the value of k_{pi} increases, the range of potential values for k_{pv} decreases.

$$\begin{cases} 0 < \gamma < 1 - \kappa \\ 0 < \kappa < 1 \end{cases} \tag{6}$$

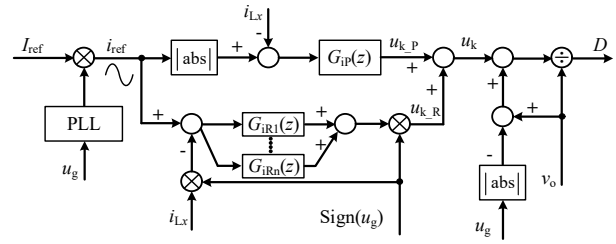

FIGURE 3. The control structure of QPR.

$$k_{pi} < \left(1 - k_{pv} \cdot \frac{T_s}{C_{dc}}\right) \cdot \frac{L_x}{T_s} \tag{7}$$

B. Internal Model-based Control Methods

The relationship in (7) shows that the trade-off between the dynamic performance of the bus voltage and the grid current is needed to be satisfied. Therefore, the internal model principle-based controllers such as quasi-proportional-resonant (QPR) controller and repetitive controller (RC) are commonly used to improve power quality under insufficient global gain.

The QPR controller is commonly used to improve tracking accuracy by increasing the gain at the fixed harmonic frequency. The PFC control structure with QPR is depicted in Fig.3, where $G_{iR}(z)$ is the transfer function of QPR and can be expressed as (8).

$$G_{iR}(z) = Z\left[\sum_{n=1}^{n} K_r \frac{2\omega_c s}{s^2 + 2\omega_c s + (n\omega_o)^2}\right] = \sum_{n=1}^{n} K_r \frac{a_n + b_n z^{-1}}{c_n + d_n z^{-1} + f_n z^{-2}} \tag{8}$$

with

$$\begin{cases} a_n = \dfrac{2\omega_c T_s}{1 + 2\omega_c T_s}, b_n = -a_n \\ d_n = \dfrac{(n\omega_o T_s)^2 - 2\omega_c T_s - 2}{1 + 2\omega_c T_s} \\ c_n = 1, f_n = \dfrac{1}{1 + 2\omega_c T_s} \end{cases} \tag{9}$$

where K_r is the resonant coefficient, ω_o is the fundamental resonant frequency, and ω_c is the cutoff frequency, n is the number of harmonic components for gain improvement.

When compensating a wide frequency band, the multiple parallel QPR controllers result in significant computational burden [28]. The phase lag introduced by the digital QPR poses challenges to system stability [29]. This contradiction between time, space, and cost is difficult to be resolved by using the linear control methods. Therefore, this paper proposes a control method that combines data model with mechanistic model to address these problems.

III. POWER QUALITY OPTIMIZATION BASED ON DATA-DRIVEN

The proposed data-driven based control structure is depicted in Fig.4. The structure consists of three main parts: the data

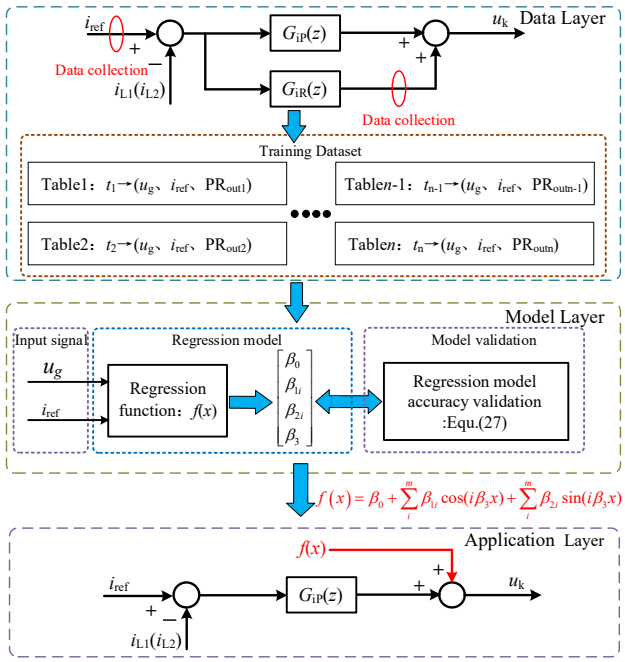

FIGURE 4. The Overall Structure of Data-Driven.

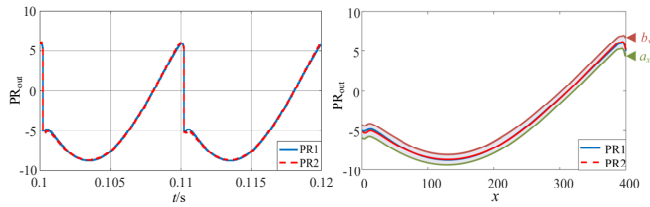

(a) (b)

FIGURE 5. Collection and preprocessing of compensation data. (a) The compensation data of PR. (b) The preprocessed compensated data of PR.

layer, the model layer, and the application layer. The data layer utilizes a control strategy based on the internal model principle, such as QPR, to control the PFC circuit. It collects the online output signals of the controller under different steady-state operating conditions to form datasets. After offline preprocessing, the datasets are fed into the model layer, where a mathematical relationship between the data and system inputs is established using nonlinear regression methods. Subsequently, at the application layer, the regression data model is integrated into the compensation loop, and combined with a low-order controller that has high stable margin, to jointly act online in the control of the PFC.

A. DATA COLLECTION AND PREPROCESSING IN THE DATA LAYER

In Fig.4, the data layer part utilizes samples to estimate the population characteristics and central limit theorem (CLT) [31] for data preprocessing. Here, the reference current i_{ref}, grid voltage u_g and the outputs of the two QPR controllers PR1 and PR2 are chosen as the data collection points. A total of 50 sets of data are collected over one steady-state fundamental cycle, under the conditions the u_g amplitude is 100V and i_{ref} amplitude is 8A. The array index j is used to represent the data collection, with a range of [1, 50]. Since the frequency of inductor current is 100Hz and the sampling frequency is 40 kHz, the range of x is [1, 400], y_x represents the compensation data corresponding to each sampling point and the data characteristics are shown in Fig.5(a). To mitigate the data error caused by disturbances and zero-crossing points as well as sampling delay, the aforementioned data is organized into a 50×400 sample matrix for preprocessing the system output data. The calculation for the sample means μ_x of the column data is given by (10).

$$\mu_x=\frac{1}{N}\sum_{j=1}^{N} y_{jx} \quad (N=50, x=1\cdots\cdots 400) \tag{10}$$

Furthermore, the sample standard deviation s_x can be obtained as

$$s_x=\sqrt{\frac{1}{N-1}\sum_{j=1}^{N}\left(y_{jx}-\mu_x\right)^2} \quad (N=50, x=1\cdots\cdots 400) \tag{11}$$

By utilizing the sample standard deviation s_x, the standard error of the data, SE_x, can be determined as

$$SE_x=\frac{s_x}{\sqrt{N}} \tag{12}$$

The confidence level represents the credibility of the sample mean being within a confidence interval, which refers to the range of statistical error in data estimation. This article establishes a confidence level of 95% and obtains the standard score g=1.96 from the standard normal distribution table. By utilizing (13), the values for the data's confidence interval [a_x, b_x] are calculated.

$$\begin{cases} a_x=\mu_x-|g|\cdot s_x \\ b_x=\mu_x+|g|\cdot s_x \end{cases} \tag{13}$$

By utilizing (13), it is possible to eliminate the abnormal data which are outside the interval [a_x, b_x], ensuring the credibility of the data. The preprocessed data characteristics are shown in Fig.5(b).

B. DATA REGRESSION AND ITS APPLICATION EVALUATION

The expression form of a data regression model is typically only limited by the imagination [30]. Therefore, considering the periodic nonlinear characteristics of the output data of the QPR controller depicted in Fig.5, this study selects the Fourier function as the nonlinear regression model, which is illustrated as

$$f(x)=\beta_0+\sum_i^l \beta_{1i}\cos(i\beta_3 x)+\sum_i^l \beta_{2i}\sin(i\beta_3 x) \tag{14}$$

where β_0, β_{1i}, β_{2i} and β_3 are the parameters that need to be regressed, and l denotes the selected function harmonics.

The expression of the regression model does not have a clear form, and there is a risk of trial and error. In order to provide a concise description of the data-driven implementation process, l=1 is used as an example for the further description.

In order to facilitate parameter estimation, (14) is equivalently transformed into (15).

$$y = f(x, \boldsymbol{\beta}) \tag{15}$$

Simultaneously, the sum of squared residuals, as expressed in (16), is introduced as the cost function to obtain the optimal regression coefficients.

$$S = \sum_{i=1}^{m} r_i^2 = \left(y_i - f(x_i, \boldsymbol{\beta})\right)^2 \quad (m = 400) \tag{16}$$

When the partial derivative of S with respect to β is equal to 0, (17) can be derived.

$$\frac{\partial S}{\partial \beta_j} = 2\sum_i r_i \frac{\partial r_i}{\partial \beta_j} = 0 \quad (j = 1, \ldots, n,\ n{=}3) \tag{17}$$

Due to the nonlinearity of the model in (14), it is not possible to obtain the regression coefficients from (17) directly. Instead, an iterative method is employed for their estimation, which is expressed as (18).

$$\beta_j \approx \beta_j^{k+1} = \beta_j^k + \Delta\beta_j \tag{18}$$

where k represents the iteration coefficient and $\Delta\boldsymbol{\beta}$ represents the iteration vector.

$f(x_i, \boldsymbol{\beta})$ is expanded by the Taylor series expansion at point $\boldsymbol{\beta}^k$

$$\begin{aligned} f(x_i, \boldsymbol{\beta}) &\approx f(x_i, \boldsymbol{\beta}^k) + \sum_j \frac{\partial f(x_i, \boldsymbol{\beta}^k)}{\partial \beta_j}\left(\beta_j - \beta_j^k\right) \\ &\approx f(x_i, \boldsymbol{\beta}^k) + \sum_j J_{ij}\Delta\beta_j \end{aligned} \tag{19}$$

where J_{ij} represents the elements of the Jacobian matrix $\mathbf{J}$.

Furthermore, the residual r_i can be derived as:

$$\begin{aligned} r_i &= y_i - f(x_i, \boldsymbol{\beta}) \\ &= \left(y_i - f(x_i, \boldsymbol{\beta}^k)\right) + \left(f(x_i, \boldsymbol{\beta}^k) - f(x_i, \boldsymbol{\beta})\right) \\ &= \Delta y_i - \sum_{j=1}^{n} J_{ij}\Delta\beta_j \end{aligned} \tag{20}$$

By substituting (20) into (17), (21) and (22) are obtained.

$$-2\sum_{i=1}^{m} J_{ij}\left(\Delta y_i - \sum_{k=1}^{n} J_{ik}\Delta\beta_k\right) = 0 \tag{21}$$

$$\sum_{i=1}^{m}\sum_{k=1}^{n} J_{ij}J_{ik}\Delta\beta_k = \sum_{i=1}^{m} J_{ij}\Delta y_i \quad (j = 1, \ldots, n,\ n{=}3) \tag{22}$$

By transforming (22) into the matrix form, it yields that:

$$\left(\mathbf{J}^{\mathrm{T}}\mathbf{J}\right)\Delta\boldsymbol{\beta} = \mathbf{J}^{\mathrm{T}}\Delta\mathbf{y} \tag{23}$$

The final iterative formula for the regression coefficients is obtained as:

$$\boldsymbol{\beta}^{(k+1)} = \boldsymbol{\beta}^{(k)} + \left(\mathbf{J}^{\mathrm{T}}\mathbf{J}\right)^{-1}\mathbf{J}^{\mathrm{T}}\mathbf{r}(\boldsymbol{\beta}^{(k)}) \tag{24}$$

By utilizing (24) to regress the model parameters, the regression models for the two parallel QPR compensation signals can be obtained, which are shown in (25) and (26).

$$\begin{aligned} f_{\mathrm{PR1}}(x) &= \beta_0 + \beta_1\cos(\beta_3 x) + \beta_2\sin(\beta_3 x) \\ &= 0.8887 - 4.792\cos(0.008082x) - 8.254\sin(0.008082x) \end{aligned} \tag{25}$$

$$\begin{aligned} f_{\mathrm{PR2}}(x) &= \beta_0 + \beta_1\cos(\beta_3 x) + \beta_2\sin(\beta_3 x) \\ &= 1.772 - 5.869\cos(0.007581x) - 8.569\sin(0.007581x) \end{aligned} \tag{26}$$

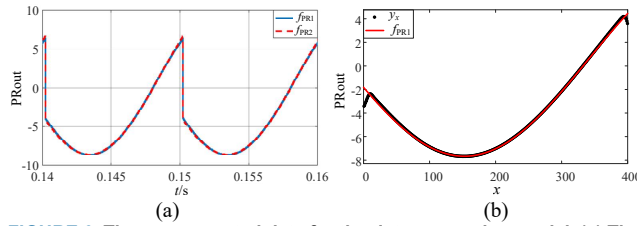

FIGURE 6. The compensated data for the data regression model. (a) The output of data regression model (b) The validation of the accuracy of data regression models.

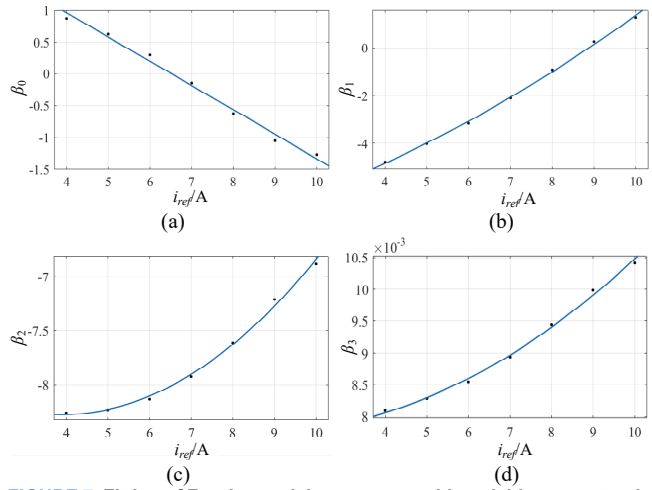

FIGURE 7. Fitting of Fourier model parameters with variable current and fixed grid voltage. (a) Fitting of β_0. (b) Fitting of β_1. (c) Fitting of β_2. (d) Fitting of β_3.

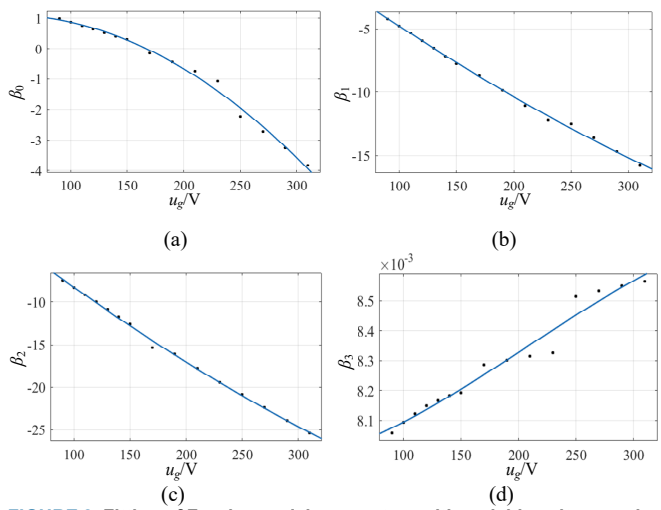

FIGURE 8. Fitting of Fourier model parameters with variable voltage and fixed current reference. (a) Fitting of β_0. (b) Fitting of β_1. (c) Fitting of β_2. (d) Fitting of β_3.

Those regression modes are depicted in Fig.6(a), and f_{PR1} is used to compare with QPR output signal within a fundamental cycle in Fig.6(b). It can be seen that the motion trends outputted by data regression model is essentially consistent with that of QPR, indicating the accuracy of data fitting during the regression process. But some fitting errors are still existed at the zero-crossing point.

To further quantify the evaluation, the coefficient of determination R^2 and root mean squared error (*RMSE*) are introduced [31], as shown in (27).

$$\begin{cases} R^2 = 1 - \dfrac{\sum_i (\hat{y}_i - y_i)^2}{\sum_i (\bar{y} - y_i)^2} = 0.9986 \\ RMSE = \sqrt{\dfrac{1}{n}\sum_{i=1}^{n} (y_i - \hat{y}_i)^2} = 0.1713 \end{cases} \tag{27}$$

where $\hat{y}_i$ is the regression predicted values, and $\bar{y}$ is the average value of the sampled data. The closer R^2 to 1, the more accurate the fitting is. And the closer *RMSE* to 0, the higher the regression accuracy. Accordingly, the independent variable can explain 99.86% of the variation in the dependent variable, and the *RMSE* value is 0.1713, which indicates that the regression model reflects accurately the QPR output information.

The above analyses are based on the regression model with the fixed values of grid voltage and current reference. To extend the applicability of the regression model, it is necessary to collect and preprocess datasets under different operating conditions.

When the amplitude of u_g is fixed, the relationship between the regression model parameters and the amplitude of the current is shown in Fig.7. With the increase of current amplitude, trajectory of β_0 shows a decreasing trend, while β_1, β_2 and β_3 exhibit an increasing trend. Similarly, Fig.8 shows the impacts of grid voltage amplitude variation on the regression model parameters when the current reference is fixed. With the increase of u_g amplitude, β_0, β_1 and β_2 show a decreasing trend, while β_3 shows an increasing trend. It is noticeable that the substantial deviations in the fitting process may arise due to the small value of β_3.

To ensure the adaptability of the parameters in (14) to changes in input information such as u_g and i_{ref}, a multivariate high-order polynomial, is constructed to describe the correlation between the parameters in (14) and the inputs of u_g and i_{ref}, as shown in (28). Since the value of β_3 is small, the 3rd-order polynomial is chosen as a base model, while the remaining parameters use the 2nd-order polynomial as a base model. In (28), k represents the regression model coefficients for β_0, β_1, β_2 and β_3. Table I presents the fitting functions for the parameters of the PR1 regression model, and similar fitting parameters can be obtained for the PR2 regression model.

$$\begin{cases} \beta_0 = k_{01}u_g^2 - k_{02}i_{ref}^2 + k_{03}u_g i_{ref} - k_{04}i_{ref} - k_{05}u_g + k_{06} \\ \beta_1 = k_{11}u_g^2 + k_{12}i_{ref}^2 + k_{13}u_g i_{ref} + k_{14}i_{ref} + k_{15}u_g - k_{16} \\ \beta_2 = k_{21}u_g^2 + k_{22}i_{ref}^2 + k_{23}u_g i_{ref} + k_{24}i_{ref} + k_{25}u_g + k_{26} \\ \beta_3 = k_{31}u_g^3 + k_{32}u_g^2 i_{ref} + k_{33}i_{ref}^2 u_g + k_{34}u_g^2 + k_{35}i_{ref}^2 \\ \qquad + k_{36}u_g i_{ref} + k_{37}i_{ref} + k_{38}u_g + k_{39} \end{cases} \tag{28}$$

Based on the data listed in Table Ⅱ, the regression results were evaluated by R^2 and *RMSE*. It can be observed that the regression equation accurately fits the parameters of the model in (14) and effectively explains the influence of the independent variables on the dependent variable. This indicates that the regression model demonstrates the adaptability to variations in grid voltage and current information and possesses accurate predictive capabilities for compensating for these variations.

TABLE I
FOURIER MODEL PARAMETER FITTING RESULTS FOR DATA PR1.

Parameter	Value	Parameter	Value	Parameter	Value
k_{01}	-6.4×10-5	k_{14}	0.9408	k_{31}	-3.6×10^{-10}
k_{02}	-0.0203	k_{15}	-0.0746	k_{32}	1.4×10^{-8}
k_{03}	0.0021	k_{16}	-1.247	k_{33}	-9.2×10^{-8}
k_{04}	-0.281	k_{21}	3.7×10^{-5}	k_{34}	1.5×10^{-7}
k_{05}	-0.0041	k_{22}	0.0253	k_{35}	2.7×10^{-5}
k_{06}	2.49	k_{23}	-0.0018	k_{36}	-5.9×10^{-6}
k_{11}	-8.3×10-5	k_{24}	0.0189	k_{37}	5.5×10^{-4}
k_{12}	0.0144	k_{25}	-0.0909	k_{38}	-1.1×10^{-5}
k_{13}	-0.0021	k_{26}	0.667	k_{39}	0.0073

TABLE II
THE EVALUATION OF FOURIER MODEL PARAMETER FITTING.

Parameter	Evaluation Metrics	Parameter	Evaluation Metrics
β_0	R^2: 0.9816 *RMSE*: 0.1606	β_2	R^2: 0.9995 *RMSE*: 0.1407
β_1	R^2: 0.9968 *RMSE*: 0.2500	β_3	R^2: 0.9577 *RMSE*: 0.0001

IV. APPLICATIONS AND ADAPTIVE ANALYSIS OF DATA-DRIVEN CONTROL

As depicted in the implementation diagram of application layer as shown in Fig.4, the regression model operates in conjunction with the forward compensation channel, ensuring that the stability of the original system loop is not compromised. Fig.9 presents the correlation between grid-side power quality and the input variables u_g and i_{ref} for three control methods using data analysis. The grid-side power quality is quantified by the total harmonic distortion (THD) of the grid current, with a universal benchmark requirement of 3% indicated by a black dashed line. The amplitude ranges are from 20V~360V for u_g and 1A~12A for i_{ref}, respectively.

When using a low-order controller, such as pure proportional controller, it is not possible to achieve satisfactory power quality, as shown in Fig.9(a). Under low current reference conditions (amplitude less than 4A), the power quality almost cannot be guaranteed throughout the entire voltage range. Even with an increase in the current reference, the THD performance in other ranges is not ideal. This is in line with the general principle in linear control systems: the lower the order of the controller, the better the system stability, but at the expense of larger steady-state tracking errors.

Fig.9(b) illustrates the THD variation trend of grid-side current under QPR control, and the THD also exhibits quadratic characteristics. Compared to the proportional control, the QPR demonstrates a wider effective range. After the implementation of data-driven compensation with pure

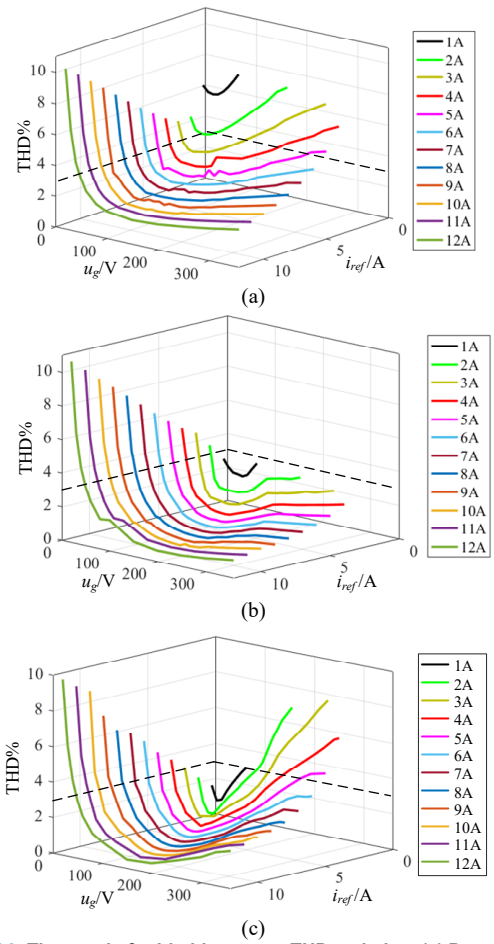

FIGURE 9. The trend of grid-side current THD variation. (a) Proportional control. (b) PR. (c) Data-driven.

proportional control, Fig.9(c) depicts the performance of grid current THD. Compared to that of QPR, the data-driven control exhibits significant superiority when u_g is low. However, its effectiveness is diminished in scenarios where u_g is large and i_{ref} is small, as well as when u_g is small and i_{ref} is large. Therefore, under high grid-side current and small grid voltage conditions, the data-driven compensation control may exhibit overcompensation and as a consequence degrade the current quality.

Fig.10 presents an alternative comparative analysis to evaluate these three controllers, with each controller's respective wireframe envelope representing the region where it satisfies the performance criteria. It is seen from Fig.10(a), that the effective range of data-driven control is significantly larger than that of the proportional control. It indicates that the data-driven control can effectively compensate for the proportional control over a wider range. However, the presence of fitting errors results in a narrower effective range compared to that of the QPR control. Simultaneously, the fitting errors can lead to over-compensation by the data-driven control when u_g is large and i_{ref} is small. Furthermore, Fig.10(b) depicts the performances of the QPR control and data-driven control. Under the condition of a smaller u_g, the

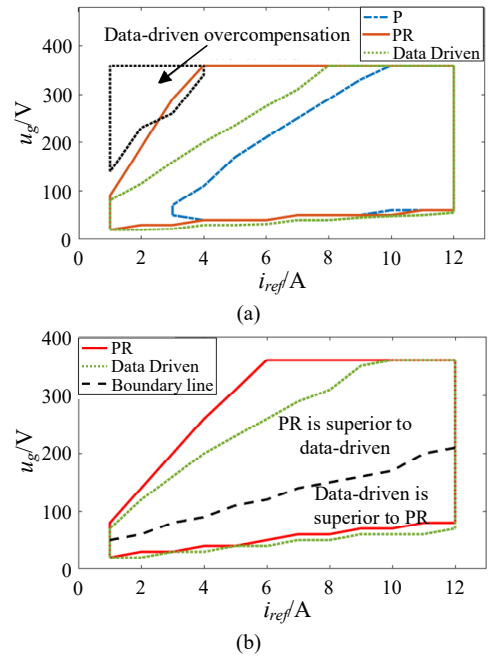

FIGURE 10. The comparison of proportional, PR, and data-driven. (a) The effective range (b) The comparison of control effects.

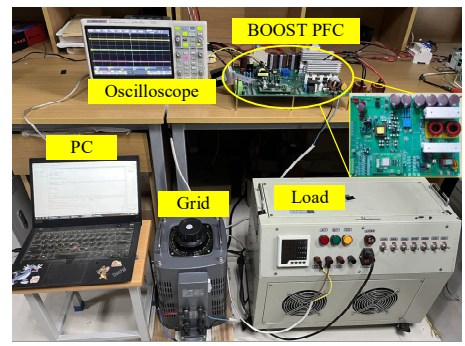

FIGURE 11. The Boost PFC experimental platform.

TABLE III
THE PARAMETERS OF EXPERIMENTAL PLATFORM.

Parameters	Values
Rated Powe P_f(kW)	5
Rated RMS value of grid voltage v_{g_rms}(V)	220
Rated RMS value of grid current i_{g_rms}(A)	23
AC voltage range (V)	50~311
DC bus voltage range (V)	350~400
Control Frequency f_c (kHz)	40
Switching Frequency f_s (kHz)	40
Initial value of inductance L_1&L_2 (mH)	1
Capacitance C_1&C_2 (μF)	4000

control effectiveness of data-driven control surpasses that of QPR control due to the omission of zero-crossing distortion data during the regression process. However, at higher u_g voltage levels, the regression errors can result in weaker control effectiveness of the data-driven control compared to the QPR control.

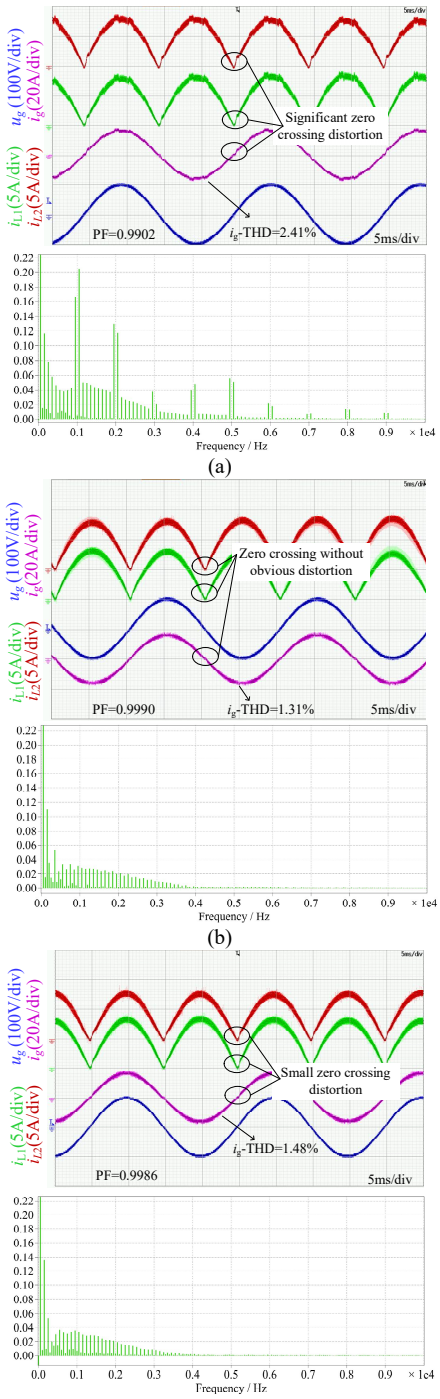

FIGURE 12. The steady-state characteristics of proportional, QPR control and data-driven control when u_g=100V and i_g=16A. (a) Proportional control. (b) QPR. (c) Data-driven.

Therefore, in terms of steady-state performance, the data-driven compensation trained by the PR control does not fully achieve the effectiveness of direct PR control. However, due to its incorporation of a smaller gain proportional control, the system exhibits a greater stable margin, allowing for further optimization of steady-state performances through improved training data for the controller. And the approach successfully improves the quality of grid current and serves as compelling evidence for the effectiveness and adaptability of data-driven control.

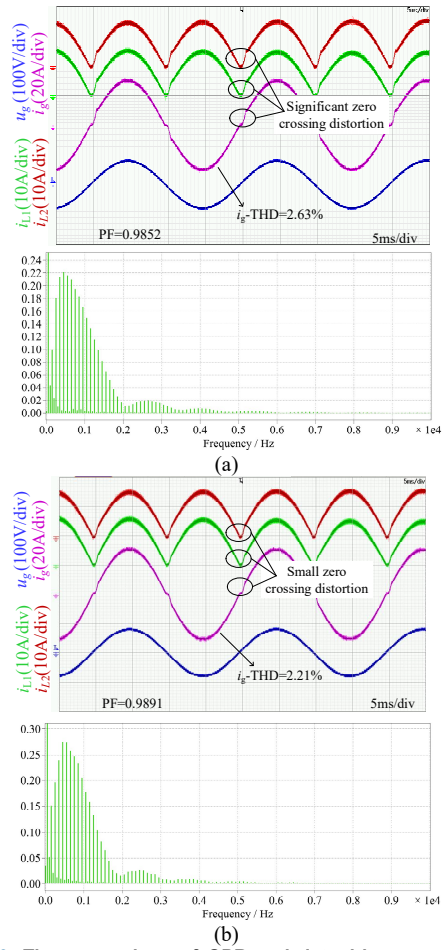

FIGURE 13. The comparison of QPR and data-driven control when u_g=80V and i_g=30A. (a) QPR. (b) Data-driven.

V. EXPERIMENTAL ANALYSIS AND VERIFICATION

In order to validate the effectiveness and feasibility of the proposed data-driven compensation control, a 5 kW IBC experimental platform is constructed in the laboratory, as depicted in Fig.11. The experimental parameters are presented in Table III.

A. COMPARISON OF STEADY-STATE CONTROL PERFORMANCES

Fig.12 depicts the steady-state characteristics of the proportional control, QPR control and data-driven compensation control. When using the proportional control, i_g is distorted significantly and its Total Harmonic Distortion (THD) is relatively high at 2.14%, with a significantly higher harmonic content compared to QPR and data-driven control. Due to the grid impedance, this distortion couples to the grid voltages at the point of common coupling, resulting in poorer power quality. By employing QPR control and data-driven compensation control, it effectively suppresses the zero-crossing distortion in i_g, u_g and i_{Lx}, thereby enhancing power quality and power factor (PF).

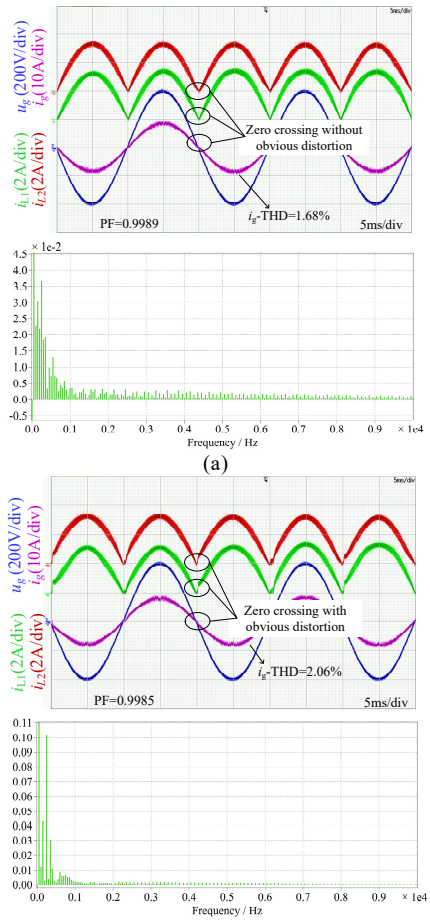

FIGURE 14. The comparison of QPR and data-driven control when u_g=400V and i_g=7A. (a) QPR. (b) Data-driven.

Fig.13 illustrates the comparison between the QPR control and data-driven compensation control for the cases of small u_g and large i_g. In this scenario, both QPR and data-driven control exhibit zero-crossing distortion issues. Furthermore, due to the omission of zero-crossing distortion data in the regression process, the THD of i_g and the power factor of the system under data-driven control are significantly better than QPR control. This indicates that in conditions of small u_g and large i_g, data-driven control demonstrates superior control performance compared to QPR control.

Fig.14 depicts the control performances of QPR and data-driven control for the cases of small i_g and large u_g. It is evident that the THD and PF of QPR control are superior to those of data-driven control, indicating that QPR control outperforms data-driven control under conditions of small i_g and large u_g. The reason behind this phenomenon lies in the significant overcompensation caused by the large fitting error in data-driven control for the cases of small i_g and large u_g, which aligns with the aforementioned theoretical analysis.

B. COMPARISON OF DYNAMIC CONTROL PERFORMANCE

Fig.15 and Fig.16 compare the dynamic response of QPR and data-driven control. It is evident that data-driven control has

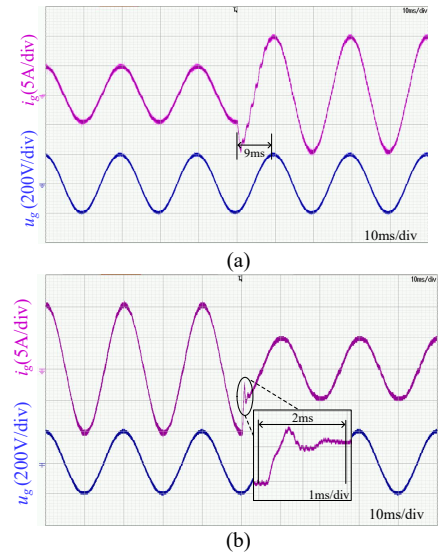

FIGURE 15. The verification of dynamic response of QPR. (a) i_{ref}=5A→10A. (b) i_{ref}=10A→5A.

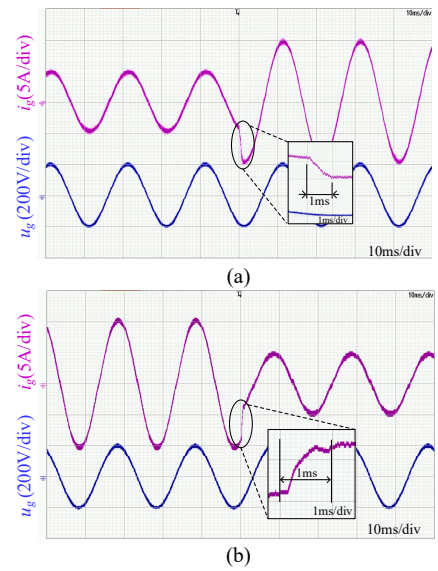

FIGURE 16. The verification of dynamic response of data-driven. (a) i_{ref}=5A→10A. (b) i_{ref}=10A→5A.

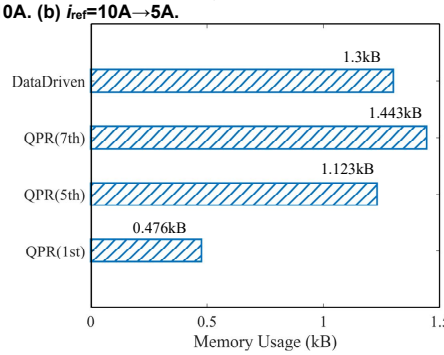

FIGURE 17. The memory usage of QPR and data-driven.

a significantly superior dynamic response compared to QPR control. Specifically, when the reference current i_{ref} increases from 5A to 10A, the adjustment time for i_g under data-driven control is approximately 1ms, whereas the distortion duration introduced by QPR control is 9ms. Conversely, when i_{ref} abruptly decreases from 10A to 5A, the adjustment time for

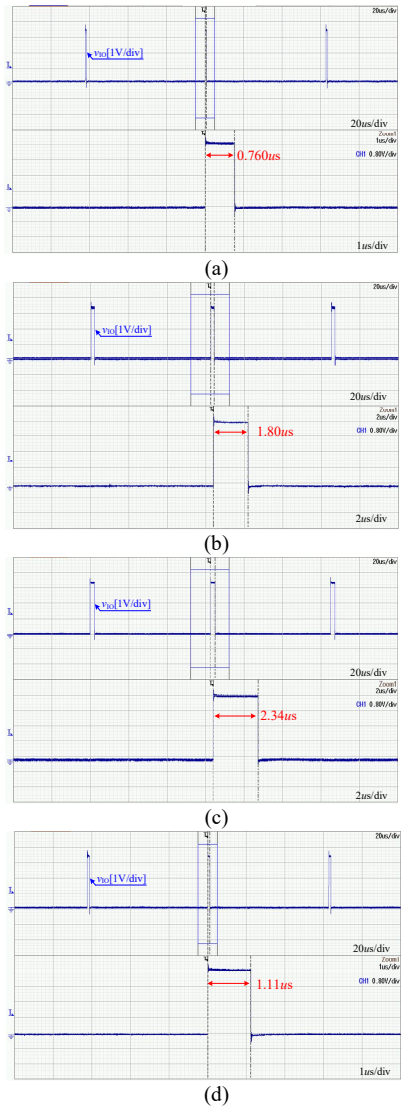

FIGURE 18. Execution time of QPR and data-driven. (a) Fundamental frequency compensation of QPR. (b) 3rd and 5th -order harmonics compensation of QPR. (c) 3rd, 5th and 7th -order harmonics compensation of QPR. (d) Data-driven.

i_g under data-driven control remains at 1ms, while the regulation time for QPR control is around 2ms, which is notably longer than that of data-driven control.

C. MEMORY USAGE AND EXECUTION TIME OF QPR AND DATA-DRIVEN

Fig.17 provides a visual comparison of the differences in memory usage between QPR control and data-driven control methods. As the order of harmonic frequencies requiring compensation increases, the memory usage of QPR control increases significantly, potentially exceeding that of data-driven control. However, data-driven control, due to its possession of a greater number of coefficients and variable definitions, results in a memory occupation of 1.3 kB.

Fig.18 illustrates a comparison of execution times between QPR and data-driven control. It is evident that as the order of harmonic frequencies compensated by QPR control increases, its execution time gradually lengthens. After compensating for the 5_{th} harmonic, the execution time is significantly longer than that of data-driven control. Although data-driven control involves more multiplication and addition/subtraction operations, its runtime remains relatively short. However, since data-driven control is derived from the output data of QPR, an increase in the QPR harmonic compensation frequency leads to changes in the output data. Nevertheless, the overall trend of QPR output remains essentially unchanged, with only minor differences in detail, thus having a relatively small impact on the data-driven model. Consequently, the variation in harmonic compensation frequency has a relatively minor effect on the memory occupation and execution time of data-driven control.

VI. CONCLUSION

This paper proposes a data-driven online compensation method to address the trade-off between control accuracy and computational complexity. The data-driven control method utilizes data from mechanism-based control methods, ensuring clear and reliable data sources. By establishing a data regression model using the multivariate nonlinear regression, the contradiction between data storage capacity and model implementation cost is effectively optimized, making it easier to program and implement. By combining the data-driven control with a feedforward channel controller, the system is compensated using the online data regression model. Compared to the traditional internal model-based control, this method has several advantages, including simplified parameter design, reduced computational complexity, a more flexible compensation range, and excellent dynamic response capability. Experimental results demonstrate that the proposed method effectively improves power quality, enhances the system's dynamic response capability, and increase the system power factor.

REFERENCES

[1] K. Yao, J. Liu, D. Zhu and Z. Jin, "High power factor CRM Boost PFC converter with optimum switching frequency variation range control based on variable inductor," *IEEE Trans. Power Electron*., vol. 36, no. 10, pp. 11019-11025, Oct. 2021.

[2] H. M. v. d. B. Campos, J. W. M. Soares, A. A. Badin and D. F. Cortez, "Single-phase hybrid switched-capacitor PFC boost rectifier with low voltage gain," *IEEE Trans. Power Electron*., vol. 38, no. 1, pp. 968-976, Jan. 2023.

[3] H. Luo, J. Xu, D. He and J. Sha, "Pulse train control strategy for CCM Boost PFC converter with improved dynamic response and unity power factor," *IEEE Trans. Ind. Electron*., vol. 67, no. 12, pp. 10377-10387, Dec. 2020.

[4] W. Yuan, Y. Wang, D. Liu, F. Deng and Z. Chen, "Impacts of inductor nonlinear characteristic in multiconverter microgrids: modeling, analysis, and mitigation," *IEEE J. Emerg. Sel. Topics Power Electron*., vol. 8, no. 4, pp. 3333-3347, Dec. 2020.

[5] H. Luo, J. Xu, Y. Luo and J. Sha, "A digital pulse train controlled high power factor DCM Boost PFC converter over a universal input voltage range," *IEEE Trans. Ind. Electron*., vol. 66, no. 4, pp. 2814-2824, Apr. 2019.

[6] Q. Zhang et al., "Output impedance modeling and high-frequency impedance shaping method for distributed bidirectional DC–DC converters in DC microgrids," *IEEE Trans. Power Electron*., vol. 35, no. 7, pp. 7001-7014, July 2020.

[7] Z. Chen, B. Liu, Y. Yang, P. Davari and H. Wang, "Bridgeless PFC topology simplification and design for performance benchmarking," *IEEE Trans. Power Electron*., vol. 36, no. 5, pp. 5398-5414, May 2021.
[8] S. Acharya and S. Mishra, "PWM control of N-Phase interleaved active front-end Boost stage-based impedance source inverter," *IEEE Trans. Power Electron*., vol. 37, no. 6, pp. 7354-7369, June 2022.
[9] H. Bodur and S. Yildirmaz, "A new ZVT snubber cell for PWM-PFC boost converter," *IEEE Trans. Ind. Electron*., vol. 64, no. 1, pp. 300–309, Jan. 2017.
[10] M. -H. Park, J. Baek, Y. Jeong and G. -W. Moon, "An interleaved totem-pole bridgeless Boost PFC converter with Soft-Switching capability adopting phase-shifting control," *IEEE Trans. Power Electron*., vol. 34, no. 11, pp. 10610-10618, Nov. 2019.
[11] S. Lu et al., "A novel single-stage AC/DC converter integrated interleaved DCM Boost PFC and LLC DC–DC with reduced bus voltage," *IEEE Trans. Ind. Electron*., vol. 71, no. 4, pp. 3525-3536, April 2024.
[12] J. Wang, H. Eto and F. Kurokawa, "Optimal zero-voltage-switching method and variable ON-Time control for predictive boundary conduction mode boost PFC converter," *IEEE Trans. Ind. Appl.,* vol. 56, no. 1, pp. 527-540, Jan.-Feb. 2020.
[13] C. Zhao and X. Wu, "Accurate operating analysis of boundary mode totem-pole Boost PFC converter considering the reverse recovery of mosfet," *IEEE Trans. Power Electron*., vol. 33, no. 12, pp. 10038-10043, Dec. 2018.
[14] Y. -S. Lai and K. -M. Ho, "Novel online parameter tuning method for digital boost PFC with transition current mode," *IEEE Trans. Ind. Appl.,* vol. 50, no. 4, pp. 2719-2727, July-Aug. 2014.
[15] Z. Chen, J. Xu, P. Davari and H. Wang, "A mixed conduction mode-controlled bridgeless Boost PFC converter and its mission profile-based reliability analysis," *IEEE Trans. Power Electron*., vol. 37, no. 8, pp. 9674-9686, Aug. 2022.
[16] M. Lee and J. -S. Lai, "Fixed-frequency hybrid conduction mode control for three-level Boost PFC converter," *IEEE Trans. Power Electron*., vol. 36, no. 7, pp. 8334-8346, July. 2021.
[17] Y. Wang, X. Ruan, Y. Leng and Y. Li, "Hysteresis current control for multilevel converter in parallel-form switch-linear hybrid envelope tracking power supply," *IEEE Trans. Power Electron*., vol. 34, no. 2, pp. 1950-1959, Feb. 2019.
[18] Z. Dong, Z. Song, W. Wang and C. Liu, "Improved zero-sequence current hysteresis control-based space vector modulation for open-end winding PMSM drives with common DC bus," *IEEE Trans. Power Electron*., vol. 70, no. 10, pp. 10755-10760, Oct. 2023.
[19] N. Tang et al., "Analog-assisted digital capacitorless low-dropout regulator supporting wide load range," *IEEE Trans. Ind. Electron*., vol. 66, no. 3, pp. 1799-1808, Mar. 2019.
[20] S. Vazquez et al., "An artificial intelligence approach for real-time tuning of weighting factors in FCS-MPC for power converters," *IEEE Trans. Ind. Electron*., vol. 69, no. 12, pp. 11987-11998, Dec. 2022.
[21] B. Long et al., "Moth–flame-optimization-based parameter estimation for FCS-MPC-controlled grid-connected converter with LCL filter," *IEEE J. Emerg. Sel. Topics Power Electron*., vol. 10, no. 4, pp. 4102-4114, Aug. 2022.
[22] A. N. Akpolat et al., "Dynamic stabilization of DC microgrids using ANN-based model predictive control," *IEEE Trans. Energy Convers*., vol. 37, no. 2, pp. 999-1010, June 2022.
[23] S. M. Seyyedzadeh and A. Shoulaie, "Accurate modeling of the nonlinear characteristic of a voltage source inverter for better performance in near zero currents," *IEEE Trans. Ind. Electron*., vol. 66, no. 1, pp. 71-78, Jan. 2019.
[24] C. Shang, M. Yang, J. Long, D. Xu, J. Zhang and J. Zhang, "An accurate VSI nonlinearity modeling and compensation method accounting for DC-Link voltage variation based on LUT," *IEEE Trans. Ind. Electron*., vol. 69, no. 9, pp. 8645-8655, Sept. 2022.
[25] R. Fernandes and O. Trescases, "A multimode 1-MHz PFC front end with digital peak current modulation," *IEEE Trans. Power Electron*., vol. 31, no. 8, pp. 5694-5708, Aug. 2016.
[26] X. Ren, Z. Guo, Y. Wu, Z. Zhang, and Q. Chen, "Adaptive LUT-based variable on-time control for CRM boost PFC converters," *IEEE Trans. Power Electron*., vol. 33, no. 9, pp. 8123–8136, Sep. 2018.
[27] Y. Wu, X. Ren, Y. Zhou, Q. Chen and Z. Zhang, "Dynamic AC line frequency response method for LUT-Based variable on-time control in 360–800Hz CRM boost PFC converter," *IEEE Trans. Power Electron*., vol. 36, no. 6, pp. 6208-6212, June 2021.
[28] Q. Zhao and Y. Ye, "A PIMR-type repetitive control for a grid-tied inverter: structure, analysis, and design," *IEEE Trans. Power Electron*., vol. 33, no. 3, pp. 2730-2739, Mar. 2018.
[29] C. Xie, X. Zhao, M. Savaghebi, L. Meng, J. M. Guerrero and J. C. Vasquez, "Multirate fractional-order repetitive control of shunt active power filter suitable for microgrid applications," *IEEE J. Emerg. Sel. Topics Power Electron*., vol. 5, no. 2, pp. 809-819, June 2017.
[30] Brunton, Steven L., and Kutz, J. Nathan. "Data-Driven Science and Engineering: Machine Learning, Dynamical Systems, and Control". Cambridge University Press, 2022.
[31] Mislick, Gregory K., and D. A. Nussbaum. "Linear Regression Analysis". World Scientific, 2015.

CONG LI received the B.S. degree in electrical engineering from the North Minzu University, Yinchuan, China, in 2017, the M.S. degree in electrical engineering from the Xi'an University of Technology, Xi'an, in 2020. He is currently working toward the Ph.D degree in electrical engineering from the Xi'an University of Technology. His research interests include modeling and control of grid converters for renewable energy systems.

QI ZHANG (Member, IEEE) received the B.S. degree in electrical engineering from the Xi'an University of Architecture and Technology, Xi'an, China, in 2004, the M.S. degree in information and control engineering and the Ph.D. degree in electrical engineering from the Xi'an University of Technology, Xi'an, in 2008 and 2012, respectively. Since 2005, he has been with the Xi'an University of Technology, where he is currently a Professor with the Department of Electrical Engineering. From 2015 to 2016, he was a Guest Researcher with Aalborg University, Aalborg, Denmark. Since 2019, he was a Postdoctoral Research Associate with Xinjiang Hope Electronic Company, Ltd. His research interests include modeling and control of power converters, bidirectional converters, and grid converters for renewable energy systems.

Rongwu Zhu (S'12-M'15-SM'22) received the B.Eng. degree in electrical engineering from Nanjing Normal University, Nanjing, China, in 2007, and the Ph.D. degree in energy technology from the Department of Energy Technology, Aalborg University, Aalborg, Denmark, in 2015. From 2011 to 2012, he was a Guest Researcher with Aalborg University. From 2016 to 2021, he was a Senior Researcher with the Chair of Power Electronics, Christian-Albrechts-University of Kiel, Kiel, Germany. He is currently a Full Professor and the Director of Department of Electrical Engineering, Harbin Institute of Technology, Shenzhen, China. He has authored and coauthored around 130 technical papers (more than 1/3 of them in international peer-reviewed journals/magazine), 20 granted and pending patents and 1 book chapter. His research interests include renewables integration, control, operation and digitalization of power electronics, and renewables-dominated grid. He served as the Editor of the International Transactions on Electrical Energy System, Associate Editor for Renewable Power Generation, Associate Editor for IEEE Open Journal of Power Electronics, and Guest Associate Editor for the IEEE Journal of Emerging and Selected Topics in Power Electronics, Guest Editor-in-Chief of the CSEE Journal of Power and Energy Systems, and Committee Chair for several International Conferences.

JiaHao Zhang was born in Xi'an, China. He received the B.Eng. degree in electrical engineering from Xi'an University of Technology, Xi'an, China, In 2022. He is currently working toward the Ph.D. degree in electrical engineering with Xi'an University of Technology, Xi'an, China. His research interests include T-type three-level inverters and research on key issues related to household energy storage.

Hui Yang, received the B.S. degree in electrical engineering from the Xi'an University of Technology, Xi an, China, in 2001, the M.S. and Ph.D. degrees in electrical engineering from the Xi'an University of Technology, Xi'an, China, in 2007 and 2018, respectively. Since 2001, she has been with Xi'an University of Technology, where she is currently an Assistant Professor with the Department of Electrical Engineering. From 2019 to 2020, she was a visiting scholar with FEEC of Virginia Tech University, USA. Her research interests include distributed power systems, digital control of power converters, and energy storage systems.

Fujin Deng (Senior Member, IEEE) received the B.Eng. degree in electrical engineering from the China University of Mining and Technology, Jiangsu, China, in 2005, the M.Sc. degree in electrical engineering from Shanghai Jiao Tong University, Shanghai, China, in 2008, and the Ph.D. degree in energy technology from the Department of Energy Technology, Aalborg University, Aalborg, Denmark, in 2012.

From 2013 to 2015 and from 2015 to 2017, he was a Postdoctoral Researcher and an Assistant Professor, respectively, with the Department of Energy Technology, Aalborg University. In 2017, he joined Southeast University, Nanjing, China, where he is currently a Professor with the School of Electrical Engineering. His main research interests include wind power generation, multilevel converters, HVDC technology, and dc grid and offshore wind farm-power systems dynamics.

Xiangdong Sun (Member, IEEE) was born in Shenyang, China, in 1971. He received the Ph.D. degree in electrical engineering from the Xi'an University of Technology, Xi'an, China, in 2003. He did the postdoctoral research with Tokyo Polytechnic University supported by the government scholarship of Japan during 2006–2008. Since 2009, he has been with the Department of Electrical Engineering, Xi'an University of Technology, where he is currently a professor. His research interests include motor control, power electronics, and renewable energy system.